Reference-input-based Imaginary Axis Current Estimation Method for DQ Control Strategy in Single-phase PWM Converters

Lin Peng, Lei Ma, *Member*, *IEEE*, Wensheng Song, *Member*, *IEEE*, and Haoran Liu

***Abstract*—For dq control strategies in single-phase pulse width modulation (PWM) converters, the β-axis current must be created by imaginary axis current estimation (IACE) methods. The estimated error of the β-axis current during the transient process causes d-q axis current loops to be incompletely decoupled, thereby affecting the dynamic performance of the current loop. The second-order generalized integrator (SOGI) method suffers from slow dynamic response. The fictive-axis emulation (FAE) method provides fast dynamic response but it is sensitive to circuit parameters. A reference-input (RI)-based IACE method is proposed to overcome the above shortcomings. According to the characteristic that the β-axis current loop has no transient process, the β-axis current is estimated by the d-q axis reference inputs. This is equivalent to introducing the β-axis reference input as a feedforward term into the d-q axis current loop, so the parameter sensitivity problem is solved, and the parameter tuning is not needed. The proposed method can maintain good steady-state performance and significantly improve the dynamic performance of the current loop. Furthermore, it is straightforward and can be easily implemented in digital controllers. Comprehensive hardware-in-the-loop (HIL) experimental comparisons with the SOGI and FAE methods have been conducted to verify the correctness and effectiveness of the proposed RI-based IACE method.**

***Index Terms*—dq control, dynamic response, imaginary axis current estimation (IACE), single-phase PWM converter.**

I. Introduction

HIGH power electric traction drive systems powered by single-phase AC power supplies are widely utilized in electric locomotive and electric multiple units (EMUs). The typical structure of EMUs is shown in Fig. 1, which includes a pantograph, a transformer, grid-side converters, traction inverters, and induction motors [1]. Nowadays, single-phase pulse width modulation (PWM) converters are the best choice for the grid-side converter due to their salient features such as energy bidirectional flow, low current harmonics, and high-power factor [2]–[4].

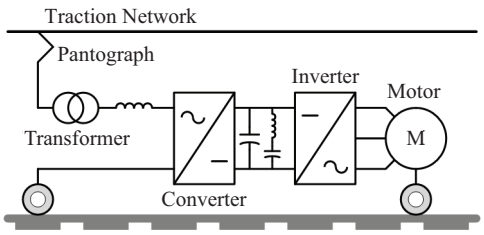

Fig. 1. Structure of high-power electric traction drive system.

Single-phase PWM converters are controlled by a classical dual closed-loop system composed of a voltage outer-loop and current inner-loop [5]. To achieve a sinusoidal line current with low harmonic distortion, various current control strategies have been proposed, such as hysteresis current control [6], proportional-resonant (PR)- and proportional-integral (PI)-based control [7]–[10], and predictive control [11]–[14]. Based on the reference frame adopted in the controller design, current control strategies can be divided into two categories: 1) stationary reference frame control [6]–[9]. 2) direct-quadrature (dq) synchronous reference frame control [10]–[17], [21]–[25], also referred to as dq control. For dq control strategies, AC sinusoidal signals are converted into DC signals using Park ($\alpha\beta$-dq) transformation. This is easy to realize indirect active (d-axis) and reactive (q-axis) current control, lower total harmonic distortion (THD), and zero steady-state error. Thus, dq control has been widely applied in PWM converters of electric traction drive systems [21], [23]–[25].

To achieve dq control in single-phase systems, β-axis signals must be created to establish the two-phase ($\alpha\beta$) stationary frame to implement the $\alpha\beta$-dq transformation [26]. dq control strategies generally assume that d-q axis current loops are completely decoupled. However, due to the β-axis current estimation error, d-q axis current loops are incompletely decoupled during the transient process, which may cause the dynamic performance of the current loop to worsen [22]. In practical applications, electric traction drive systems need good steady-state performance and faster dynamic response to deal with frequent switching between light and heavy loads. Therefore, the performance of the imaginary axis current estimation (IACE) method is vital.

Diverse techniques are employed to estimate the β-axis

Manuscript received August 23, 2020; revised November 25, 2020; accepted March 4, 2021. Date of online publication May 6, 2022; date of current version July 4, 2024. This work was supported by the National Natural Science Foundation of China under Grant 61733015, 62473322, and High-Speed Railway Joint Funds of National Natural Science Foundation of China under Grant U1934204.

L. Peng is with the School of Electrical Engineering, Sichuan Polytechnic University, Deyang 618000, China.

L. Ma (corresponding author, email: malei@swjtu.edu.cn), W. S. Song, and H. R. Liu are with the School of Electrical Engineering, Southwest Jiaotong University, Chengdu 611756, China.

DOI: 10.17775/CSEEJPES.2020.04220

2096-0042 © 2020 CSEE. This is an open access article under the CC BY-NC-ND license (http://creativecommons.org/licenses/by-nc-nd/4.0/).

current, such as transport delay [15], Hilbert transformation [16], all-pass filter [17], second-order generalized integrator (SOGI) [14], [18]–[21], and fictive-axis emulation (FAE) [22]. Transport delay is simple to implement, but has poor dynamic performance and large storage space requirements, so it is generally used in low-power applications. Hilbert transformation is very sensitive to input disturbances and frequency fluctuation. An all-pass filter requires a large amount of calculation and its dynamic response is slow. SOGI has good performance and is easily implemented in digital controllers, which provides two types of filters with 0 dB gain at the fundamental frequency. The band-pass filter is used to obtain the fundamental component of the input signal. The low-pass filter (LPF) is used to obtain the quadrature component of the input signal, which belongs to a popular quadrature signal generation (QSG) technology. SOGI is a good choice for obtaining the quadrature component of the grid-side voltage, but its dynamic response is still slower for the current loop. FAE is used to calculate the β-axis estimated current through the β-axis closed-loop of the real system. Compared with SOGI, FAE delivers faster dynamic performance and is easier to understand, but it has the disadvantage of parameter sensitivity [22].

To overcome the shortcomings of conventional IACE methods and improve the dynamic performance of the current loop, a reference-input (RI)-based IACE method is proposed in this paper. The major contributions are as follows. First, the incomplete decoupling model of the current loop in the dq frame is given. Second, according to the analysis of this model, it is concluded that IACE methods will affect the dynamic performance of the current loop. Third, the β-axis current is estimated by the d-q axis reference inputs according to the characteristic that the β-axis current loop has no transient process. This is equivalent to introducing the β-axis reference current as a feedforward term into the d-q axis current loop, thereby reducing the settling time of the current loop and suppressing the overshoot of the line current. The proposed method is not only insensitive to circuit parameters but also does not need parameter tuning. Furthermore, it is simple and easily implemented in digital controllers.

The rest of this paper is organized as follows. In Section II, the mathematical model of a single-phase PWM converter is briefly reviewed, and an incomplete decoupling model of the current loop in the dq frame is presented. The analysis shows IACE methods primarily affect the dynamic performance of the current loop. In Section III, the influence of the conventional methods, such as SOGI and FAE on the dynamic performance of the current loop, is analyzed based on the incomplete decoupling model. The RI-based IACE method is proposed in Section IV. Section V evaluates the performance of the proposed method based on a hardware-in-the-loop (HIL) simulation platform and compares it with SOGI and FAE methods. The conclusion is presented in Section VI.

II. System Description

A. Complete Decoupling Model of dq Current Control

The equivalent circuit topology of single-phase two-level PWM converters in locomotive traction systems is illustrated in Fig. 2 [23]–[25], where $u_{\rm s}$ and $i_{\rm s}$ are the grid-side voltage and the line current, respectively.L and R are the equivalent inductance and resistance of the grid-side, respectively. $u_{\rm ab}$ is the input voltage of the H-bridge composed of four power switching devices S_1–S_4.$R_{\rm L}$ and $C_{\rm d}$ are the equivalent resistance load and buffer capacitance of the DC-link, respectively. The series resonance filter composed of the filter inductance L_2 and filter capacitor C_2 is used to absorb the low-frequency harmonic of the DC-link voltage $u_{\rm dc}$.

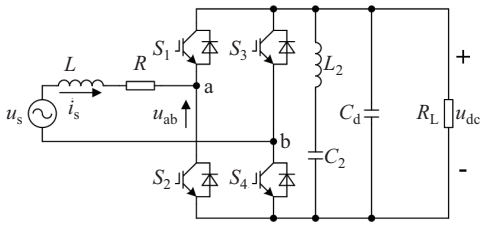

Fig. 2. Circuit topology of the adopted PWM converter.

The mathematical model in the dq frame of the adopted system is expressed as [22]:

$$\begin{bmatrix} u_{{\rm ab}d} \\ u_{{\rm ab}q} \end{bmatrix} = \begin{bmatrix} u_{{\rm s}d} \\ u_{{\rm s}q} \end{bmatrix} - \begin{bmatrix} R & -\omega L \\ \omega L & R \end{bmatrix} \begin{bmatrix} i_{{\rm s}d} \\ i_{{\rm s}q} \end{bmatrix} - L \begin{bmatrix} \frac{{\rm d}i_{{\rm s}d}}{{\rm d}t} \\ \frac{{\rm d}i_{{\rm s}q}}{{\rm d}t} \end{bmatrix} \tag{1}$$

where $u_{{\rm s}d}$, $i_{{\rm s}d}$ and $u_{{\rm ab}d}$ are the d-axis components of $u_{\rm s}$, $i_{\rm s}$, and $u_{\rm ab}$, respectively. $u_{{\rm s}q}$, $i_{{\rm s}q}$ and $u_{{\rm ab}q}$ are the q-axis components of $u_{\rm s}$, $i_{\rm s}$ and $u_{\rm ab}$, respectively. ω is the fundamental angular frequency of $u_{\rm s}$. There are typical coupling terms $\omega L i_{{\rm s}q}$ and $-\omega L i_{{\rm s}d}$ in (1).

A voltage feedforward decoupling method was proposed in [22] to realize dq decoupling control, and its mathematical model is expressed as:

$$\begin{bmatrix} u_{{\rm ab}d} \\ u_{{\rm ab}q} \end{bmatrix} = \begin{bmatrix} u_{{\rm s}d} \\ u_{{\rm s}q} \end{bmatrix} + \omega L \begin{bmatrix} i_{{\rm s}q} \\ -i_{{\rm s}d} \end{bmatrix} - G_{\rm c}(s) \begin{bmatrix} i_{d{\rm ref}} - i_{{\rm s}d} \\ i_{q{\rm ref}} - i_{{\rm s}q} \end{bmatrix} \tag{2}$$

where $i_{d{\rm ref}}$ and $i_{q{\rm ref}}$ are the d-q axis reference inputs. $u_{{\rm s}d}/u_{{\rm s}q}$ and $\omega L i_{{\rm s}q}/-\omega L i_{{\rm s}d}$ are the feedforward terms, respectively. $G_{\rm c}$ is the transfer function of the controller.

In dq decoupling control strategies, it is assumed that the coupling terms in (1) can be eliminated by the feedforward terms in (2) at any time, then the complete decoupling control can be achieved [10]–[17], [21]–[25]. Substituting (2) into (1), the transfer function of the adopted system is derived as:

$$P(s) = \frac{1}{Ls + R} \tag{3}$$

Combining (1)–(3), the block diagram of the current loop with the complete decoupling model is shown in Fig. 3, and its closed-loop transfer function $G_{\rm o}(s)$ is:

$$G_{\rm o}(s) = \frac{i_{{\rm s}d}(s)}{i_{d{\rm ref}}(s)} = \frac{i_{{\rm s}q}(s)}{i_{q{\rm ref}}(s)} = \frac{G_{\rm c}(s)P(s)}{1 + G_{\rm c}(s)P(s)} \tag{4}$$

B. Incomplete Decoupling Model of dq Current Control

Due to the estimation error of β-axis signals, the coupling

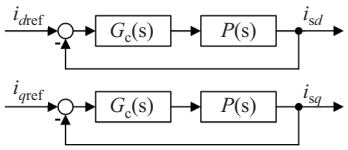

Fig. 3. Block diagram of the current loop with complete decoupling model.

terms in (1) cannot be completely eliminated by the feedforward terms in (2), especially in the transient process [22]. Considering that the grid-side voltage $u_{\rm s}$ is the reference vector, $u_{{\rm s}d}$ and $u_{{\rm s}q}$ can be expressed as:

$$\begin{cases} u_{{\rm s}d} = u_{\rm sm} \\ u_{{\rm s}q} = 0 \end{cases} \tag{5}$$

where $u_{\rm sm}$ is the peak value of $u_{\rm s}$.

Since the fundamental frequency of $u_{\rm s}$ is much smaller than the switching frequency, $u_{{\rm s}d}$ and $u_{{\rm s}q}$ can be regarded as constants in one switching period. Furthermore, from (1) and (2), $u_{{\rm s}d}$ and $u_{{\rm s}q}$ are not coupled. Therefore, $u_{{\rm s}d}$ and $u_{{\rm s}q}$ in (1) and (2) can be eliminated by the voltage feedforward method. However, the d-q axis currents $i_{{\rm s}d}$ and $i_{{\rm s}q}$ in (1) and (2) are coupled so that they will affect each other. When the β-axis current estimation error is large, the influence of the estimation error of the β-axis current on the current loop cannot be ignored.

Assume that the d-q axis estimated currents in (2) are $i_{{\rm se}d}$ and $i_{{\rm se}q}$, while the actual currents in (1) are represented by $i_{{\rm s}d}$ and $i_{{\rm s}q}$, respectively. Equation (2) can then be expressed as:

$$\begin{bmatrix} u_{{\rm ab}d} \\ u_{{\rm ab}q} \end{bmatrix} = \begin{bmatrix} u_{{\rm s}d} \\ u_{{\rm s}q} \end{bmatrix} + \omega L \begin{bmatrix} i_{{\rm se}q} \\ -i_{{\rm se}d} \end{bmatrix} - G_{\rm c}(s) \begin{bmatrix} i_{d\rm ref} - i_{{\rm se}d} \\ i_{q\rm ref} - i_{{\rm se}q} \end{bmatrix} \tag{6}$$

Combining (1), (3)–(6) and then simplifying, the incomplete decoupling model of the current loop is derived as:

$$\begin{aligned} \begin{bmatrix} i_{{\rm se}d} \\ i_{{\rm se}q} \end{bmatrix} = G_{\rm o}(s) \begin{bmatrix} i_{d\rm ref} \\ i_{q\rm ref} \end{bmatrix} + G_{\delta}(s) \begin{bmatrix} \delta_{{\rm i}q}(s) \\ \delta_{{\rm i}d}(s) \end{bmatrix} \\ + G_{\delta 1}(s) \begin{bmatrix} i_{d\rm ref} - i_{{\rm se}d} \\ i_{q\rm ref} - i_{{\rm se}q} \end{bmatrix} \end{aligned} \tag{7}$$

where $\delta_{{\rm i}d}$ and $\delta_{{\rm i}q}$ are disturbances caused by d-q axis current errors. G_{δ} is the closed-loop transfer function from disturbances ($\delta_{{\rm i}q}/\delta_{{\rm i}d}$) to the estimated current ($i_{{\rm se}d}/i_{{\rm se}q}$). $G_{\delta 1}$ is the closed-loop transfer function from the errors ($i_{d\rm ref} - i_{{\rm se}d}/i_{q\rm ref} - i_{{\rm se}q}$) between the reference inputs and the estimated currents to the estimated current ($i_{{\rm se}d}/i_{{\rm se}q}$).

$\delta_{{\rm i}d}$, $\delta_{{\rm i}q}$, G_{δ}, and $G_{\delta 1}$ in (7) are defined as:

$$\begin{cases} \delta_{{\rm i}d} = -\omega L(i_{{\rm s}d} - i_{{\rm se}d}) \\ \delta_{{\rm i}q} = \omega L(i_{{\rm s}q} - i_{{\rm se}q}) \\ G_{\delta}(s) = \dfrac{i_{{\rm se}d}(s)}{\delta_{{\rm i}q}(s)} = \dfrac{i_{{\rm se}q}(s)}{\delta_{{\rm i}d}(s)} = \dfrac{P(s)}{1 + G_{\rm c}(s)P(s)} \\ G_{\delta 1}(s) = \dfrac{i_{{\rm se}d}(s)}{i_{d\rm ref} - i_{{\rm se}d}} = \dfrac{i_{{\rm se}q}(s)}{i_{q\rm ref} - i_{{\rm se}q}} = \dfrac{1}{1 + G_{\rm c}(s)P(s)} \end{cases} \tag{8}$$

It is reasonable to assume that a stabilizing controller $G_{\rm c}$ exists and provides a fast-dynamic response, and the adopted IACE method has good stead-stated performance. Then, the gain of $G_{\delta 1}$ in (8) will be much smaller than 0 dB, the terms in (7) related to $G_{\delta 1}$ can be ignored, so (7) can be simplified as:

$$\begin{bmatrix} i_{{\rm se}d}(s) \\ i_{{\rm se}q}(s) \end{bmatrix} = G_{\rm o}(s) \begin{bmatrix} i_{d\rm ref}(s) \\ i_{d\rm ref}(s) \end{bmatrix} + G_{\delta}(s) \begin{bmatrix} \delta_{{\rm i}q}(s) \\ \delta_{{\rm i}d}(s) \end{bmatrix} \tag{9}$$

The block diagram of the current loop with the incomplete decoupling model is illustrated in Fig. 4.

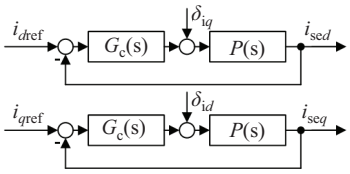

Fig. 4. Block diagram of the current loop with incomplete decoupling model.

Similarly, the gain of G_{δ} in (8) will be larger than zero and smaller than 0 dB, so the terms in (7) related to G_{δ} can be ignored only when the disturbances $\delta_{{\rm i}q}$ and $\delta_{{\rm i}d}$ are small.

In steady-state, $\delta_{{\rm i}q}$ and $\delta_{{\rm i}d}$ are very small, the current loop can be characterized by (4), so the steady-state performance of the current loop is determined by the current controller $G_{\rm c}$.

During the transient process, $\delta_{{\rm i}q}$ and $\delta_{{\rm i}d}$ will become larger because of the influence of the dynamic characteristics of the adopted IACE method. According to classical control theory [27], when the trend of $\delta_{{\rm i}q}$ and $\delta_{{\rm i}d}$ is consistent with that of the reference inputs $i_{d\rm ref}$ and $i_{q\rm ref}$, the changing rate of the controlled signal will increase, otherwise, it will decrease. These two results can be described as:

$$\begin{cases} \delta_{{\rm i}q} \uparrow, i_{d\rm ref} \uparrow \quad \text{or} \quad \delta_{{\rm i}q} \downarrow, i_{d\rm ref} \downarrow \Rightarrow \dfrac{{\rm d}i_{{\rm se}d}}{{\rm d}t} \uparrow \\ \delta_{{\rm i}d} \uparrow, i_{q\rm ref} \uparrow \quad \text{or} \quad \delta_{{\rm i}q} \downarrow, i_{d\rm ref} \downarrow \Rightarrow \dfrac{{\rm d}i_{{\rm se}q}}{{\rm d}t} \uparrow \end{cases} \Rightarrow \frac{{\rm d}i_{\rm s}}{{\rm d}t} \uparrow \tag{10}$$

$$\begin{cases} \delta_{{\rm i}q} \downarrow, i_{d\rm ref} \uparrow \quad \text{or} \quad \delta_{{\rm i}q} \uparrow, i_{d\rm ref} \downarrow \Rightarrow \dfrac{{\rm d}i_{{\rm se}d}}{{\rm d}t} \downarrow \\ \delta_{{\rm i}d} \downarrow, i_{q\rm ref} \uparrow \quad \text{or} \quad \delta_{{\rm i}q} \uparrow, i_{d\rm ref} \downarrow \Rightarrow \dfrac{{\rm d}i_{{\rm se}q}}{{\rm d}t} \downarrow \end{cases} \Rightarrow \frac{{\rm d}i_{\rm s}}{{\rm d}t} \downarrow \tag{11}$$

where ${\rm d}i_{{\rm se}d}/{\rm d}t$, ${\rm d}i_{{\rm se}q}/{\rm d}t$, and ${\rm d}i_{\rm s}/{\rm d}t$ represent the changing rate of $i_{{\rm se}d}$, $i_{{\rm se}q}$, and $i_{\rm s}$, respectively. Therefore, the dynamic characteristic of IACE methods primarily affects the dynamic performance of the current loop.

III. Performance Analysis of Conventional IACE Methods

The d-q axis estimated currents $i_{{\rm se}d}$ and $i_{{\rm se}q}$ are obtained by α-β axis currents, and are expressed as:

$$\begin{bmatrix} i_{{\rm se}d} \\ i_{{\rm se}q} \end{bmatrix} = \begin{bmatrix} \cos\omega t & \sin\omega t \\ -\sin\omega t & \cos\omega t \end{bmatrix} \begin{bmatrix} i_{{\rm s}\alpha} \\ i_{{\rm se}\beta} \end{bmatrix} \tag{12}$$

where $i_{{\rm s}\alpha}$ is the line current $i_{\rm s}$. $i_{{\rm se}\beta}$ is the β-axis estimated component of $i_{\rm s}$, which is obtained by IACE methods.

To simplify the analysis, it is assumed that the adopted converter is operating as a rectifier with a unit power factor, and only the amplitude error between the β-axis actual current

$i_{s\beta}$ and $i_{se\beta}$ is considered. The α-β axis currents can be expressed as:

$$\begin{cases} i_{s\alpha} = I_{sm}\cos\omega t \\ i_{s\beta} = I_{sm}\sin\omega t \\ i_{se\beta} = (I_{sm} + \Delta I_{sm})\sin\omega t \end{cases} \tag{13}$$

where I_{sm} is the peak value of i_s. ΔI_{sm} is the peak error.

Substituting (13) into (12), i_{sed} and i_{seq} are derived as:

$$\begin{cases} i_{sed} = I_{sm} + \dfrac{1}{2}\Delta I_{sm}(1-\cos 2\omega t) \\ i_{seq} = \dfrac{1}{2}\Delta I_{sm}\sin 2\omega t \end{cases} \tag{14}$$

There are double-frequency components in i_{sed} and i_{seq} when ΔI_{sm} is not zero. This will cause i_{sed} and i_{seq} to increase or decrease.

Since the controllers have the same dynamic performance at all times, the performance of the IACE methods can be studied in any quadrant. In the subsequent description, the same simulation condition is adopted for discussion to compare the performance of IACE methods. The electrical parameters of the adopted converter are listed in Table I, which are the actual parameters of China Railways High-speed 3 (CRH $_3$) type EMUs [9]. The dynamic simulation waveforms are shown in Fig. 5, where i_{sref} and $i_{\beta ref}$ are the α-β axis reference currents, respectively. At the same instant in the 4th quadrant, the q-axis reference input i_{qref} equals zero, the d-axis reference input i_{dref} rises from 1095 A to 2190 A.

TABLE I
ELECTRICAL PARAMETERS OF THE ADOPTED SYSTEM

Parameters	Values
Grid-side voltage RMS value (u_s)	1550 V
Grid-side inductance (L)	2.2 mH
Grid-side resistance (R)	0.068 Ω
Grid-side fundamental frequency(f_0)	50 Hz
DC-link reference voltage ($U_{dc\text{-}ref}$)	3000 V
DC-link buffer capacitance (C_d)	3000 μF
DC-link resonant filter inductance (L_2)	0.83 mH
DC-link resonant filter capacitance (C_2)	3000 μF
Switching frequency (f_{pwm})	1.25 kHz
DC-link rated current	400 A
Grid-side rated line current	1095 A

A. SOGI Method

The transfer function of SOGI used to estimate the β-axis current is [18]:

$$i_{se\beta}(s) = \frac{k\omega^2}{s^2 + k\omega s + \omega^2} i_s(s) \tag{15}$$

where k is the damping factor. The line current i_s is the input signal of the SOGI block. Since the transfer function in (15) is an LPF with a phase shift of 90-degree, $i_{se\beta}$ is the quadrature component of i_s and is insensitive to circuit parameters. The settling time of SOGI depends on the selection of k, and its minimum value occurs with $k = 1.57$ at about 15 ms [19]. Compared with the current controller, the settling time of SOGI is longer. Therefore, $i_{se\beta}$ will change slower than $i_{s\beta}$ during the transient process, which means that ΔI_{sm} in (14)

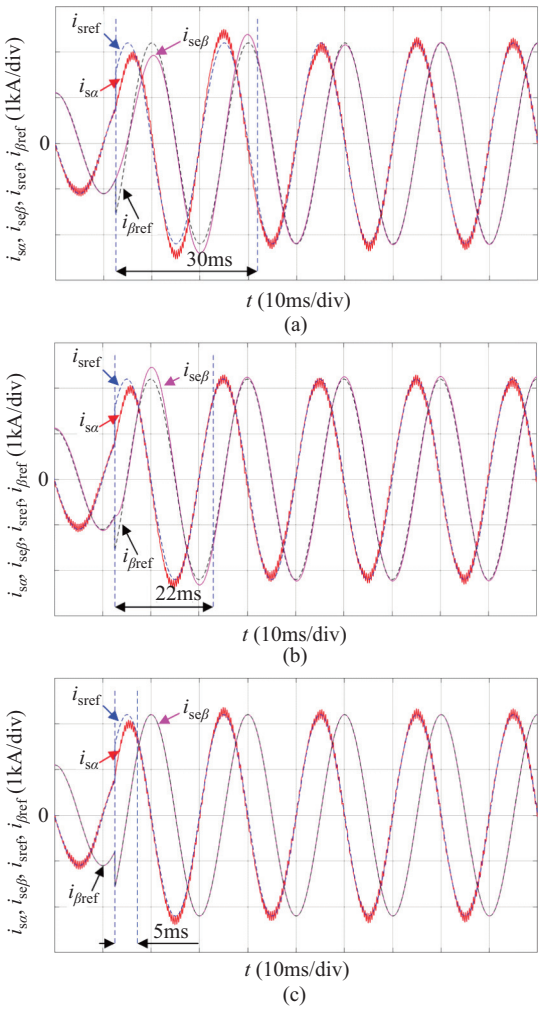

Fig. 5. Dynamic simulation waveforms with different IACE methods when i_{dref} rises from 1095 A to 2190 A. (a) SOGI. (b) FAE. (c) RI-based IACE.

is smaller than zero when i_{dref} rises. In the 4th quadrant, the following results can be obtained:

$$\begin{cases} \Delta I_{sm} < 0 \\ 0 < \cos 2\omega t \le 1 \\ -1 < \sin 2\omega t \le 0 \end{cases} \Rightarrow \begin{cases} i_{sed} < i_{sd} \\ i_{seq} > i_{sq} = 0 \end{cases}$$
$$\Rightarrow \begin{cases} \delta_{id} \le 0 \\ \delta_{iq} \le 0 \end{cases} \Rightarrow \begin{cases} \delta_{id} \downarrow \\ \delta_{iq} \downarrow \end{cases} \tag{16}$$

From (16), the trend of δ_{iq}/δ_{id} is opposite to that of i_{dref}/i_{qref}. According to (11), the changing rate $\mathrm{d}i_s/\mathrm{d}t$ of i_s will decrease, so the settling time of the current loop will be longer.

In Fig. 5(a), about 4 ms after i_{dref} is changed, i_s is close to i_{sref}, but $i_{se\beta}$ is still smaller than $i_{\beta ref}$. When i_s and $i_{se\beta}$ are both close to their reference inputs, δ_{iq} and δ_{id} are reduced to a negligible amount, and the system enters a new steady-state at about 30 ms.

In summary, the dynamic response of SOGI is slower than that of the current controller, resulting in the deterioration of the dynamic performance of the current loop.

B. FAE Method

The transfer function of FAE is [22]:

$$i_{\mathrm{se}\beta}(s) = \frac{1}{Ls+R}[u_{\mathrm{s}\beta}(s) - u_{\mathrm{ab}\beta}(s)] \tag{17}$$

where $u_{\mathrm{s}\beta}$ and $u_{\mathrm{ab}\beta}$ are the β-axis components of u_{s} and u_{ab}, respectively. Among them, $u_{\mathrm{ab}\beta}$ is obtained by the inverse Park (dq-$\alpha\beta$) transformation of $u_{\mathrm{ab}d}$ and $u_{\mathrm{ab}q}$, and all variables are the β-axis components of the real variables.

Comparing (3) and (17), the transfer function of the FAE block and the system are the same. From this, a closed-loop system is established in the β-axis, which runs synchronously with the real system. For the nominal system, $i_{\mathrm{se}\beta}$ can be changed synchronously with i_{s}. Therefore, the dynamic response of FAE is faster than that of SOGI.

Since FAE has no control delay caused by the PWM module, $i_{\mathrm{se}\beta}$ will change faster than $i_{\mathrm{s}\beta}$ during the transient process. Therefore, ΔI_{sm} in (14) will be larger than zero when $i_{d\mathrm{ref}}$ rises. In the 4th quadrant, the following results can be obtained:

$$\begin{cases} \Delta I_{\mathrm{sm}} > 0 \\ 0 < \cos 2\omega t \le 1 \\ -1 < \sin 2\omega t \le 0 \end{cases} \Rightarrow \begin{cases} i_{\mathrm{se}d} > i_{\mathrm{s}d} \\ i_{\mathrm{se}q} < i_{\mathrm{s}q} = 0 \end{cases}$$
$$\Rightarrow \begin{cases} \delta_{\mathrm{i}d} \ge 0 \\ \delta_{\mathrm{i}q} \ge 0 \end{cases} \Rightarrow \begin{cases} \delta_{\mathrm{i}d} \uparrow \\ \delta_{\mathrm{i}q} \uparrow \end{cases} \tag{18}$$

From (18), the trend of $\delta_{\mathrm{i}q}/\delta_{\mathrm{i}d}$ is consistent with that of $i_{d\mathrm{ref}}/i_{q\mathrm{ref}}$. According to (10), the changing rate $\mathrm{d}i_{\mathrm{s}}/\mathrm{d}t$ of i_{s} will increase, so the settling time of the current loop will be shorter.

In Fig. 5(b), about 4 ms after $i_{d\mathrm{ref}}$ is changed, i_{s} is close to i_{sref}, but $i_{\mathrm{se}\beta}$ is still larger than $i_{\beta\mathrm{ref}}$. When i_{s} and $i_{\mathrm{se}\beta}$ are both close to their reference input currents, the system enters a new steady-state at about 22 ms.

From (17), $i_{\mathrm{se}\beta}$ depends on $u_{\mathrm{s}\beta}$, $u_{\mathrm{ab}\beta}$, R, and L, so the FAE method has the disadvantage of parameter sensitivity. This issue has been studied in [22], and the following is only a brief review:

Let R_{FAE} and L_{FAE} represent the nominal values of R and L in (17), respectively. When the circuit parameters are mismatched, the current controller must provide a double-frequency component, which is expressed as a complex vector $\boldsymbol{u}_{\mathrm{ab}dq}$:

$$\boldsymbol{u}_{\mathrm{ab}dq} = \left(\frac{R-R_{\mathrm{FAE}}}{2} - \mathrm{j}\omega\frac{L-L_{\mathrm{FAE}}}{2}\right) I_{\mathrm{s}dq}\mathrm{e}^{-\mathrm{j}2\omega t} \tag{19}$$

where $I_{\mathrm{s}dq}$ is the complex amplitude in the dq frame of i_{s}. However, conventional current controllers do not support this, so the harmonic component of i_{s} will increase. Since R is much smaller than L, the current harmonic component is primarily caused by inductance mismatch.

In short, the dynamic response of FAE is faster than that of the current controller, which will reduce the settling time of the current loop. However, FAE is sensitive to circuit parameters, therefore, an online inductance parameter estimation is necessary to ensure the estimated accuracy of $i_{\mathrm{s}\beta}$ in practical applications. This will increase the programming complexity.

IV. Reference-Input-Based Imaginary Axis Current Estimation Method

For dq control strategies of single-phase PWM converters, the equivalent structure of the current loop in the $\alpha\beta$ frame is shown in Fig. 6, where $u_{\mathrm{s}\beta}$, $i_{\mathrm{s}\beta}$ and $u_{\mathrm{ab}\beta}$ are the β-axis components of the grid-side voltage $u_{\mathrm{s}\alpha}$, line current $i_{\mathrm{s}\alpha}$, and H bridge input voltage $u_{\mathrm{ab}\alpha}$, respectively.

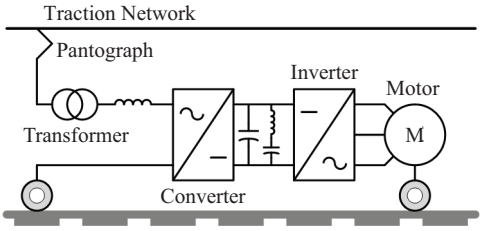

Fig. 6. Equivalent structure of the current loop in the $\alpha\beta$ frame.

From the analysis in Section II, $u_{\mathrm{s}\beta}$ and $i_{\mathrm{s}\beta}$ need to be created. The dq-axis components $u_{\mathrm{s}d}$ and $u_{\mathrm{s}q}$ of u_{s} are independent of the current loop and can be eliminated by the voltage feedforward. This means that QSG technology is a good choice for $u_{\mathrm{s}\beta}$. In addition, the $\alpha\beta$-dq or dq-$\alpha\beta$ transformation needs the angular frequency ω of u_{s}. To reduce the computational burden, signal synchronization technology can be used to simultaneously obtain t$u_{\mathrm{s}\beta}$ and ω, such as SOGI-PLL [19]. For IACE methods, QSG technology is not the only solution, the study in [22] provides a good idea.

In the steady-state, the relationship between the d-q axis estimated currents $i_{\mathrm{se}d}/i_{\mathrm{se}q}$, the d-q axis currents $i_{\mathrm{s}d}/i_{\mathrm{s}q}$ and the d-q axis reference inputs $i_{d\mathrm{ref}}/i_{q\mathrm{ref}}$ are:

$$\begin{cases} i_{\mathrm{se}d} = i_{\mathrm{s}d} = i_{d\mathrm{ref}} \\ i_{\mathrm{se}q} = i_{\mathrm{s}q} = i_{q\mathrm{ref}} \end{cases} \tag{20}$$

Applying the dq-$\alpha\beta$ transformation to (20), the β-axis current $i_{\mathrm{s}\beta}$ is:

$$i_{\mathrm{s}\beta} = i_{\mathrm{se}\beta} = i_{\beta\mathrm{ref}} = i_{d\mathrm{ref}}\sin(\omega t) + i_{q\mathrm{ref}}\cos(\omega t) \tag{21}$$

where $i_{\mathrm{se}\beta}$ is the β-axis estimated current. $i_{\beta\mathrm{ref}}$ is the β-axis reference input.

In Fig. 6, $i_{\mathrm{s}\alpha}$ is the controlled object, and its change is limited by the real system. In contrast, the β-axis current loop is fictitious, so $i_{\mathrm{s}\beta}$ is not limited by the real system. This means that there is no transient process for the β-axis current loop, $i_{\mathrm{s}\beta}$ can be set to change synchronously with $i_{\beta\mathrm{ref}}$. From this, the proposed method uses (21) to calculate $i_{\mathrm{s}\beta}$, so it is called the RI-based IACE method.

Obviously, the proposed method is effective in the steady-state. During the transient process, its rationality is analyzed as follows:

First, the PWM modulator updates the switching state of the power devices according to the switching period. Assuming that there is no current error during the transient process, the current loop can enter a steady state after a few switching periods. This provides the possibility of taking (21) as an IACE method.

Secondly, $i_{\mathrm{se}\beta}$ obtained by (21) is the target value of $i_{\mathrm{s}\beta}$ during the transient process, and $i_{\mathrm{s}\alpha}$ is still obtained by the current sensor. This is equivalent to introducing $i_{\beta\mathrm{ref}}$ into the d-q axis current loop as a feedforward term. The feedforward control strategy is to perform open-loop compensation according to the disturbance or the change of the reference input, it not only can improve the system performance and suppress disturbance but also will not change the close-loop characteristics of the system [28], [29], so the proposed method has a theoretical basis.

Thirdly, when the reference current changes, $i_{\mathrm{se}\beta}$ obtained by (21) can reach the steady-state target value in one control period. The influence of the estimation error of $i_{\mathrm{se}\beta}$ on the current loop is analyzed as follows:

With the same simulation condition set in Section III, ΔI_{sm} in (14) is larger than zero when the line current i_{s} is smaller than i_{sref}, otherwise, ΔI_{sm} is smaller than or equal to zero. In the 4th quadrant, ΔI_{sm} is larger than zero when i_{sref} rises. The following results can be obtained:

$$\begin{cases} \Delta I_{\mathrm{sm}} > 0 \\ 0 < \cos 2\omega t \le 1 \\ -1 < \sin 2\omega t \le 0 \end{cases} \Rightarrow \begin{cases} i_{sed} > i_{sd} \\ i_{seq} < i_{sq} = 0 \end{cases}$$
$$\Rightarrow \begin{cases} \delta_{\mathrm{i}d} \ge 0 \\ \delta_{\mathrm{i}q} \ge 0 \end{cases} \Rightarrow \begin{cases} \delta_{\mathrm{i}d} \uparrow \\ \delta_{\mathrm{i}q} \uparrow \end{cases} \tag{22}$$

This situation is the same as (18), but a comparison between (17) and (21) shows that ΔI_{sm} in (22) is larger than ΔI_{sm} in (18). Therefore, compared with FAE, the changing rate $\mathrm{d}i_{\mathrm{s}}/\mathrm{d}t$ of i_{s} will increase faster, and the settling time of the current loop will be shorter. As shown in Fig. 5(c), about 5 ms after $i_{d\mathrm{ref}}$ is changed, both i_{s} and $i_{\mathrm{se}\beta}$ are close to their reference inputs, and the system enters a new steady-state.

Assume that i_{s} is overshoot, that is, ΔI_{sm} is smaller than zero, then the following results can be obtained:

$$\begin{cases} \Delta I_{\mathrm{sm}} < 0 \\ 0 < \cos 2\omega t \le 1 \\ -1 < \sin 2\omega t \le 0 \end{cases} \Rightarrow \begin{cases} i_{sed} < i_{sd} \\ i_{seq} < i_{sq} = 0 \end{cases}$$
$$\Rightarrow \begin{cases} \delta_{\mathrm{i}d} \le 0 \\ \delta_{\mathrm{i}q} \le 0 \end{cases} \Rightarrow \begin{cases} \delta_{\mathrm{i}d} \downarrow \\ \delta_{\mathrm{i}q} \downarrow \end{cases} \tag{23}$$

This situation is the same as (16), the changing rate of i_{s} will be reduced and will become closer to i_{sref} much faster. Therefore, the overshoot of i_{s} can be suppressed.

According to the control period T_{c} of the current loop, the discrete expression of $i_{\mathrm{se}\beta}$ in (21) is derived as:

$$i_{\mathrm{se}\beta}(k) = i_{d\mathrm{ref}}(k)\sin(\omega k T_{\mathrm{c}}) + i_{q\mathrm{ref}}(k)\cos(\omega k T_{\mathrm{c}}) \tag{24}$$

When the converter works as a rectifier with the unit power factor, $i_{\mathrm{se}\beta}(k)$ can be simplified as follows:

$$i_{\mathrm{se}\beta}(k) = i_{d\mathrm{ref}}(k)\sin(\omega k T_{\mathrm{c}}) \tag{25}$$

The block diagram of the proposed method is shown in Fig. 7, where ω is obtained by the existing PLL block. $i_{d\mathrm{ref}}$ is the output of the voltage loop, $i_{q\mathrm{ref}}$ is generally a constant. These variables only need the values at the kth control instant, which are independent of circuit parameters and do not need to be tuned.

V. HIL Experimental Verification

A hardware-in-the-loop (HIL) experimental platform is constructed to evaluate the correctness and effectiveness of the proposed RI-based IACE method, and the test results are compared with the conventional SOGI and FAE methods. The photograph of the HIL platform is shown in Fig. 8, where the power loop is realized in a MicroLabBox real-time simulator. The C program of the control strategy runs in the TMS320F28335 digital signal processor (DSP). The electrical parameters of the experimental system are listed in Table I, and the control block diagram is shown in Fig. 9, where the

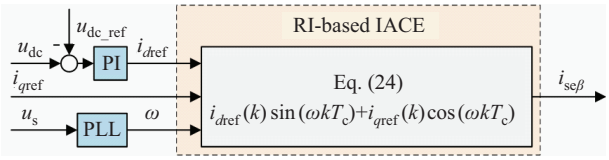

Fig. 7. Block diagram of the proposed RI-based IACE method.

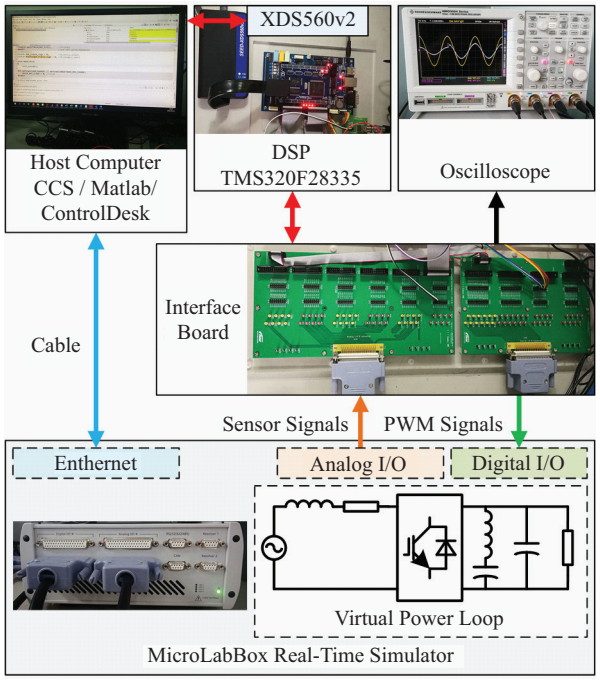

Fig. 8. Block diagram of the HIL experimental platform.

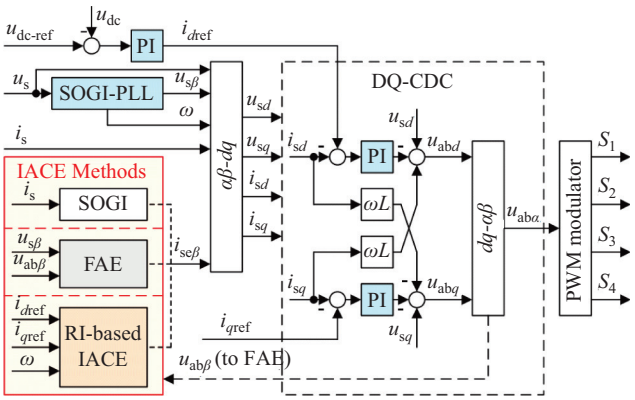

Fig. 9. Control block diagram of the experimental system.

control strategy selects the dq current decoupling control (DQ-CDC). DQ-CDC has been widely applied in the traction drive system [21], [23]–[25]. The PI parameters of controllers have been well-tuned according to system performance when the IACE method is SOGI, and remain unchanged throughout the experiment.

A. Steady-state Performance

The adopted converter works as a rectifier when the rated load and the proposed IACE method are used, and the steady-state experimental waveforms and the line current FFT analysis result are shown in Fig. 10, where $u_{\rm s}$ and $i_{\rm s}$ are the grid-side voltage and the line current, respectively. $u_{\rm dc}$ is the DC-link voltage.

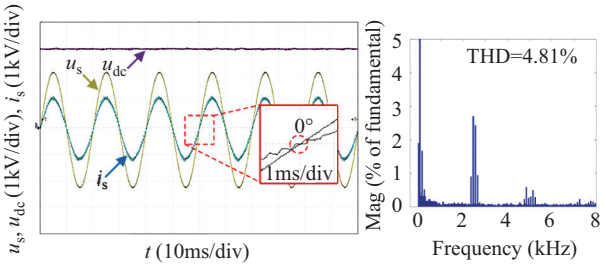

Fig. 10. Steady-state experimental waveforms and line current FFT analysis of the proposed method.

SOGI and FAE, as IACE methods, have been verified in [14] and [22], respectively, and both can provide good steady-state performance. In Fig. 10, $i_{\rm s}$ is sinusoidal and in phase with $u_{\rm s}$. The line current THD value is about 4.81%, which is close to the line current THD values (4.95%, 4.80%) with the SOGI and FAE methods.

The steady-state experiment verifies that the steady-state performance of the current loop is primarily determined by current controllers.

B. Transient Process Performance

The dynamic experimental waveforms with different IACE methods under d- or q-axis reference current $i_{d\rm ref}/i_{q\rm ref}$ step-change conditions are shown in Figs. 11 and 12, respectively, where $u_{\rm s}$ and $i_{\rm s}$ are the grid-side voltage and the line current, respectively. $i_{\rm sref}$ is the α-axis reference current.

In Fig. 11, $i_{q\rm ref}$ is set to zero, and $i_{d\rm ref}$ increases from 1095 A to 2190 A. The settling time of the current loop with SOGI, FAE, and the proposed RI-based IACE method are about 21 ms, 16 ms, and 2 ms, respectively. Among them, the settling time, using the proposed method, is the shortest, and using SOGI, it is the longest.

In Fig. 12, $i_{d\rm ref}$ is set to 1095 A, and $i_{q\rm ref}$ increases from 0 A to 1095 A. The settling time of the current loop with SOGI, FAE, and the proposed method are 22 ms, 19 ms, and 2 ms, respectively. Among them, the settling time using the proposed method is still the shortest, and using SOGI, it is the longest.

Comparing the trend of $i_{\rm s}$ and $i_{\rm sref}$ during the transient process in Figs. 11 and 12, the overshoot of $i_{\rm s}$ is the largest when the IACE method is SOGI. In contrast, the overshoot

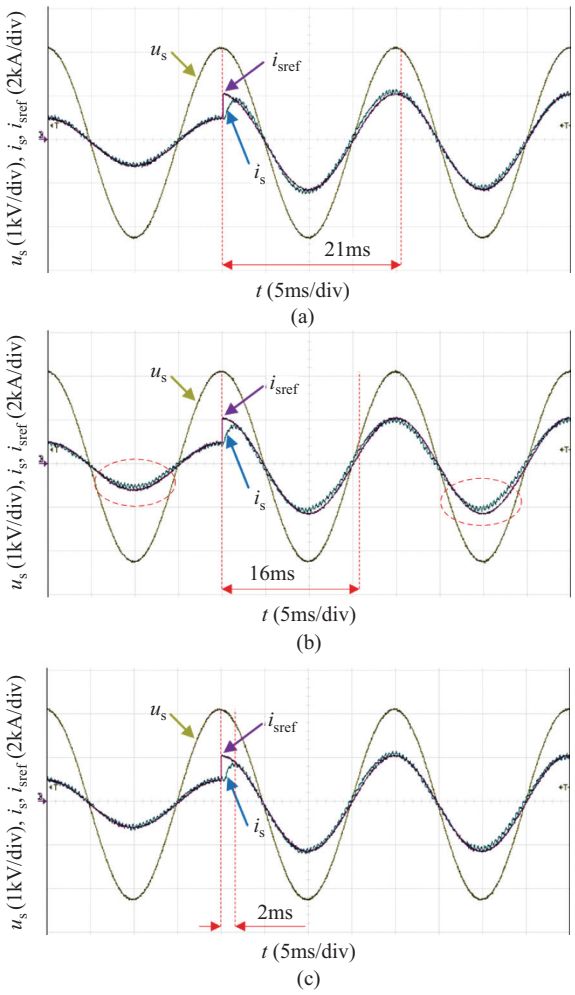

Fig. 11. Dynamic experimental waveforms with different IACE methods when $i_{d\rm ref}$ rises from 1095 A to 2190 A. (a) SOGI. (b) FAE. (c) RI-based IACE.

of $i_{\rm s}$ is almost zero, the smallest when the proposed RI-based IACE method is adopted.

In addition, from (17), the β-axis estimated current $i_{{\rm se}\beta}$ with the FEA method is related to the β-axis component $u_{{\rm ab}\beta}$ of the output of the current controller. The accuracy of $u_{{\rm ab}\beta}$ is determined by the switching frequency of the converter, signal measurement error, and current loop control accuracy. The experimental verifications in [12] and [22] show that the FAE method can obtain good results in high switching frequency and low-power applications. However, from the experimental waveforms of the FAE method in Fig. 11(b) and Fig. 12(b), there still is a large difference between the peak value of $i_{\rm sref}$ and $i_{\rm s}$ in the steady-state. Therefore, in low frequency and high-power applications, the FAE method has shortcomings even in the nominal system, and therefore, online inductance parameter identification is necessary.

The experimental results of SOGI, FAE, and the proposed RI-based IACE method are shown in Table II. The excellent performance of the proposed RI-based IACE method is verified from aspects of computational burden, programming complexity, algorithm characteristics, and steady-state and dynamic characteristics. From the system performance, the

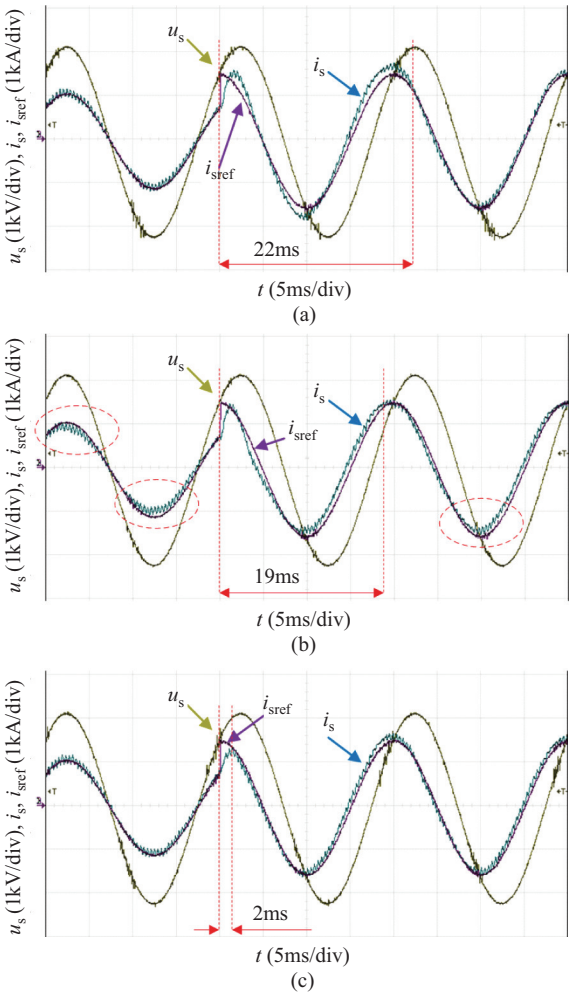

Fig. 12. Dynamic experimental waveforms with different IACE methods when i_{qref} rises from 0 A to 1095 A. (a) SOGI. (b) FAE. (c) RI-based IACE.

TABLE II
EXPERIMENTAL RESULTS OF THE THREE IACE METHODS

Performance	SOGI	FAE	RI-based IACE
Computational burden	5 μs	1.8 μs	1.6 μs
Programming complexity	Complex	Normal	Easy
Sensitivity to inductance	No	Yes	No
Parameter tuning	Yes	No	No
Line current THD value	4.95%	4.80%	4.81%
Settling time of current loop	22 ms	19 ms	2 ms
Overshoot of line current	Large	Large	Small

three methods have similar steady-state performance. When the adopted IACE method is the proposed method, the settling time and the overshoot of the line current are the smallest during the transient process. Moreover, the proposed method does not need tune parameters and is insensitive to circuit parameters, so it can provide a simpler and better-performance solution for estimating the β-axis current. Since the theoretical analysis in Section II is based on a general model, the proposed method can also be applied to other control schemes or circuit topologies in single-phase PWM converters based on dq control strategies.

VI. CONCLUSION

A reference-input (RI)-based IACE method for dq control strategies of single-phase PWM converters has been proposed. Due to the estimated error of the β-axis current obtained by IACE methods, d-q axis current loops are incompletely decoupled. In this paper, First, the incomplete decoupling model of the current loop is given. From the analysis of this model, it can be concluded that IACE methods primarily affect the dynamic characteristics of the current loop. Secondly, since the β-axis current loop has the characteristic of no transient process, the proposed method used the d-q axis reference inputs to estimate the β-axis current, which can simplify the calculation and improve the dynamic performance of the current loop. Finally, the effectiveness and correctness of the proposed method were evaluated on a HIL experimental platform. Compared with conventional SOGI and FAE methods, the proposed RI-based IACE method has the following salient features:

1) Compared with the FAE method, it is insensitive to circuit parameters.

2) Compared with the SOGI method, it does not need parameter tuning.

3) Compared with the SOGI and FAE methods, it can effectively improve the dynamic performance of the current loop. Also, it is simple and easily implemented in digital controllers.

REFERENCES

[1] H. B. Cui, W. S. Song, X. L. Ge, and X. Y. Feng, "High-frequency resonance suppression of high-speed railways in China," *IET Electrical Systems in Transportation*, vol. 6, no. 2, pp. 88–95, Jun. 2016.

[2] C. Y. Gu, Z. D. Zheng, L. Xu, K. Wang, and Y. D. Li, "Modeling and control of a multiport power electronic transformer (PET) for electric traction applications," *IEEE Transactions on Power Electronics*, vol. 31, no. 2, pp. 915–927, Feb. 2016.

[3] Q. M. Xu, F. J. Ma, Z. X. He, Y. D. Chen, J. M. Guerrero, A. Luo, Y. Li, and Y. F. Yue, "Analysis and comparison of modular railway power conditioner for high-speed railway traction system," *IEEE Transactions on Power Electronics*, vol. 32, no. 8, pp. 6031–6048, Aug. 2017.

[4] Y. Hong, Y. Li, Z. Shuai and H. Yang, "Low-Frequency Stability Analysis of Power Electronic Traction Transformer Based Train-Network System," *CSEE Journal of Power and Energy Systems*, vol. 10, no. 4, pp. 1608–1617, Jul. 2024.

[5] A. Chatterjee and K. B. Mohanty, "Current control strategies for single phase grid integrated inverters for photovoltaic applications-a review," *Renewable and Sustainable Energy Reviews*, vol. 92, pp. 554–569, May 2018.

[6] P. A. Dahono, "New hysteresis current controller for single-phase full-bridge inverters," *IET Power Electronics*, vol. 2, no. 5, pp. 585–594, Sep. 2009.

[7] D. N. Zmood and D. G. Holmes, "Stationary frame current regulation of PWM inverters with zero steady-state error," *IEEE Transactions on Power Electronics*, vol. 18, no. 3, pp. 814–822, May 2003.

[8] M. Brenna, F. Foiadelli, and D. Zaninelli, "New stability analysis for tuning PI controller of power converters in railway application," *IEEE Transactions on Industrial Electronics*, vol. 58, no. 2, pp. 533–543, Feb. 2011.

[9] C. X. Zhang, S. R. Yu, and X. L. Ge, "A stationary-frame current vector control strategy for single-phase PWM rectifier," *IEEE Transactions on Vehicular Technology*, vol. 68, no. 3, pp. 2640–2651, Mar. 2019.

[10] B. Bahrani, S. Kenzelmann, and A. Rufer, "Multivariable-PI-based dq current control of voltage source converters with superior axis decoupling capability," *IEEE Transactions on Industrial Electronics*, vol. 58, no. 7, pp. 3016–3026, Jul. 2011.

[11] S. Kwak, S. E. Kim, and J. C. Park, "Predictive current control methods with reduced current errors and ripples for single-phase voltage source inverters," *IEEE Transactions on Industrial Informatics*, vol. 11, no. 5, pp. 1006–1016, Oct. 2015.
[12] J. P. Ma, W. S. Song, X. F. Wang, F. Blaabjerg, and X. Y. Feng, "Low-complexity model predictive control of single-phase three-level rectifiers with unbalanced load," *IEEE Transactions on Power Electronics*, vol. 33, no. 10, pp. 8936–8947, Oct. 2018.
[13] W. S. Song, J. P. Ma, L. Zhou, and X. Y. Feng, "Deadbeat predictive power control of single-phase three-level neutral-point-clamped converters using space-vector modulation for electric railway traction," *IEEE Transactions on Power Electronics*, vol. 31, no. 1, pp. 721–732. Jan. 2016.
[14] W. S. Song, Z. X. Deng, S. L. Wang, and X. Y. Feng, "A simple model predictive power control strategy for single-phase PWM converters with modulation function optimization," *IEEE Transactions on Power Electronics*, vol. 31, no. 7, pp. 5279–5289, Jul. 2016.
[15] U. A. Miranda, L. G. B. Rolim, and M. Aredes, "A DQ synchronous reference frame current control for single-phase converters," in *2005 IEEE 36th Power Electronics Specialists Conference*, 2005, pp. 1377–1381.
[16] M. Saitou and T. Shimizu, "Generalized theory of instantaneous active and reactive powers in single-phase circuits based on Hilbert transform," in *Proceedings of IEEE Annual IEEE Power Electronics Specialists Conference*, Cairns, Qld, Australia, 2002, pp. 1419–1424.
[17] R. Y. Kim, S. Y. Choi, and I. Y. Suh, "Instantaneous control of average power for grid tie inverter using single phase D-Q rotating frame with all pass filter," in *30th Annual Conference of IEEE Industrial Electronics Society, 2004. IECON 2004*, Busan, Korea (South), 2004, pp. 274–279.
[18] M. Ciobotaru, R. Teodorescu, and F. Blaabjerg, "A new single-phase PLL structure based on second order generalized integrator," in *2006 37th IEEE Power Electronics Specialists Conference*, Jeju, 2006, pp. 1–6.
[19] A. Kulkarni and V. John, "A novel design method for SOGI-PLL for minimum settling time and low unit vector distortion," in *IECON 2013–39th Annual Conference of the IEEE Industrial Electronics Society*, Vienna, 2013, pp. 274–279.
[20] S. Golestan, J. M. Guerrero, F. Musavi, and J. C. Vasquez, "Single-phase frequency-locked loops: a comprehensive review," *IEEE Transactions on Power Electronics*, vol. 34, no. 12, pp. 11791–11812, Dec. 2019.
[21] Y. C. Liao, Z. G. Liu, H. Zhang, and B. Wen, "Low-frequency stability analysis of single-phase system with *dq*-Frame impedance approach—Part I: impedance modeling and verification," *IEEE Transactions on Industry Applications*, vol. 54, no. 5, pp. 4999–5011, Sep./Oct. 2018.
[22] B. Bahrani, A. Rufer, S. Kenzelmann, and L. A. C. Lopes, "Vector control of single-phase voltage-source converters based on fictive-axis emulation," *IEEE Transactions on Industry Applications*, vol. 47, no. 2, pp. 831–840, Mar./Apr. 2011.
[23] H. Wang, W. Mingli, and J. J. Sun, "Analysis of low-frequency oscillation in electric railways based on small-signal modeling of vehicle-grid system in *dq* frame," *IEEE Transactions on Power Electronics*, vol. 30, no. 9, pp. 5318–5330, Sep. 2015.
[24] Y. C. Liao, Z. G. Liu, G. N. Zhang, and C. Xiang, "Vehicle-grid system modeling and stability analysis with forbidden region-based criterion," *IEEE Transactions on Power Electronics*, vol. 32, no. 5, pp. 3499–3512, May 2017.
[25] K. T. Jiang, C. X. Zhang, and X. L. Ge, "Low-frequency oscillation analysis of the train-grid system based on an improved forbidden-region criterion," *IEEE Transactions on Industry Applications*, vol. 54, no. 5, pp. 5064–5073, Sep./Oct. 2018.
[26] J. Xu, H. Qian, S. Bian, Y. Hu and S. Xie, "Comparative study of single-phase phase-locked loops for grid-connected inverters under non-ideal grid conditions," *CSEE Journal of Power and Energy Systems*, vol. 8, no. 1, pp. 155–164, Jan. 2022.
[27] G. F. Franklin, J. D. Powell, and A. Emami-Naeini, *Feedback Control of Dynamic Systems*, 6th ed., Pearson Higher Education, Inc., 2010.
[28] E. Prempain and I. Postlethwaite, "Feedforward control: a full-information approach," *Automatica*, vol. 37, no. 1, pp. 17–28, Jan. 2001.
[29] L. Liu, S. Y. Tian, D. Y. Xue, T. Zhang, and Y. Q. Chen, "Industrial feedforward control technology: a review," *Journal of Intelligent Manufacturing*, vol. 30, no. 8, pp. 2819–2833, Dec. 2019.

Lin Peng received a B.S. degree in Communication Engineering from the University of Electronic Science and Technology of China, Chengdu, China, in 2006, and an M.Eng. degree in Control Engineering from Chongqing University, Chongqing, China, in 2011, and a Ph.D. degree in Electrical Engineering at Southwest Jiaotong University, Chengdu, China, in 2022. He is currently an associate Professor with the School of Electrical Engineering, Sichuan Polytechnic University, Deyang, China. His research interests include modeling and controlling power converters in railway traction drive systems.

Lei Ma received a B.Eng. degree in Automatic Control from Chongqing University, Chongqing, China, in 1993, an M.Sc. degree in Electrical Engineering from Southwest Jiaotong University, Chengdu, China, in 1996, and the Dr.-Ing. degree in Electrical Engineering from Ruhr University Bochum, Bochum, Germany, in 2006. From 2006 to 2009, he was an Assistant Professor with the Department of Robotics and Telematics, University of Würzburg, and also the Deputy Director and Member of the Board of Supervisors with the Zentrum für Telematik e.V.,Würzburg, Germany. Since September 2009, he has been a Professor with the School of Electrical Engineering, Southwest Jiaotong University. His research interests include control theory with applications to robotics, renewable energy, and rail transit systems.

Wensheng Song received a B.S. degree in Electronic and Information Engineering and a Ph.D. degree in Electrical Engineering from Southwest Jiaotong University, Chengdu, China, in 2006 and 2011, respectively. From September 2009 to September 2010, he was a Visiting Scholar with the Department of Electrical Engineering and Computer Science, University of California at Irvine, Irvine, CA, USA. From July 2015 to December 2015, he was a Visiting Scholar with the University of Alberta, Edmonton, AB, Canada. He is currently a Full Professor with the School of Electrical Engineering, Southwest Jiaotong University. His current research interests include digital control and modulation methods of electrical AC-DC-AC railway traction drive systems and multilevel converters.

Haoran Liu received a B.S. degree in Electrical Engineering and Automation from Panzhihua University, Panzhihua, China, in 2015, and an M.S. degree in Computer Application Technology from Central South University of Forestry and Technology, Changsha, China, in 2018. He is currently pursuing a Ph.D. degree in Electrical Engineering with the school of Electrical Engineering, Southwest Jiaotong University, Chengdu, China. His research interests include robust control and modulation of power converters in railway applications.